Since January 2020 Elsevier has created a COVID-19 resource centre with free information in English and Mandarin on the novel coronavirus COVID-19. The COVID-19 resource centre is hosted on Elsevier Connect, the company's public news and information website.

Environmental Research 210 (2022) 112899

Contents lists available at ScienceDirect

Environmental Research

journal homepage: www.elsevier.com/locate/envres

Pollution characteristics and sources of environmentally persistent free radicals and oxidation potential in fine particulate matter related to city lockdown (CLD) in Xi'an, China

Dyussenova Ainur [a], Qingcai Chen [a,*], Yuqin Wang [a], Hao Li [a], Hao Lin [a], Xuying Ma [b], Xin Xu [c]

[a] School of Environmental Science and Engineering, Shaanxi University of Science and Technology, Xi'an, 710021, China
[b] College of Geomatics, Xi'an University of Science and Technology, Xi'an, 710054, China
[c] Xi'an Institute for Innovative Earth Environment Research, Xi'an, 710061, China

ARTICLE INFO

Keywords:
COVID-19
$PM_{2.5}$
Environmentally persistent free radicals (EPFRs)
Oxidation potential (OP)
Sources

ABSTRACT

The impact of COVID-19 control on air quality have been prevalent for the past two years, however few studies have explored the toxicity of atmospheric particulate matter during the epidemic control. Therefore, this research highlights the characteristics and sources of oxidative potential (OP) and the new health risk substances environmentally persistent free radicals (EPFRs) in comparison to city lockdown (CLD) with early days of 2019–2020. Daily particulate matter ($PM_{2.5}$) samples were collected from January 14 to February 3, 2020, with the same period during 2019 in Xi'an city. The results indicated that the average concentration of $PM_{2.5}$ decreased by 48% during CLD. Concentrations of other air pollutants and components, such as PM_{10}, NO_2, SO_2, WSIs, OC and EC were also decreased by 22%, 19%, 2%, 17%, 6%, and 4% respectively during the CLD, compared to the same period in 2019. Whereas only O_3 increased by 30% during CLD. The concentrations of EPFRs in $PM_{2.5}$ was considerably lower than in 2019, which decreased by 12% during CLD. However, the OP level was increased slightly during CLD. Moreover, both EPFRs/PM and DTTv/PM did not decrease or even increase significantly, manifesting that the toxicity of particulate matter has not been reduced by more gains during the CLD. Based on PMF analysis, during the epidemic period, the contribution of traffic emission is significantly reduced, while EPFRs and DTTv increased, which consist of significant O_3 and secondary aerosols. This research leads to able future research on human health effect of EPFRs and oxidative potential and can be also used to formulate the majors to control EPFRs and OP emissions, suggest the need for further studies on the secondary processing of EPFRs and OP during the lockdown period in Xi'an. .The COVID-19 lockdown had a significant impact on both social and economic aspects. The city lockdown, however, had a positive impact on the environment and improved air quality, however, no significant health benefits were observed in Xi'an, China.

1. Introduction

The presence of fine particulate matter ($PM_{2.5}$) in the atmosphere adversely affects human health by inducing reactive oxygen species (ROS) production. ROS are oxygen-containing substances with higher oxidative toxicity. Studies have shown that the environmentally persistent free radicals (EPFRs) likewise contain single electron such as oxygen-containing or oxygen-centered EPFRs, and recently has been analyzed as long-lasting and hazardous substances (Qian et al., 2020; Zhu et al., 2019). The catalysis mechanism of EPFRs continuously converts O_2 molecules into reactive oxygen species (ROS), indicated as one of the mechanisms underlying health problems (Chen et al., 2018b; Vejerano et al., 2018). Furthermore, toxic products damage the human lungs by deposition in the respiratory system or enhancing the ROS level (Xu et al., 2020). In general, a toxicological mechanism is oxidative stress caused by excessive accumulation of oxidative potential (OP) in the human body. Therefore, characterizing the sources is an essential need to control the production process and minimize their adverse impact on our environment. Previous studies have highlighted the origin of atmospheric $PM_{2.5}$ and EPFRs by primary sources and secondary sources. The primary sources include cigarette tar, various fly ashes, biomass, automobile exhaust, and coal combustion; secondary sources

* Corresponding author. School of Environmental Science and Engineering, Shaanxi University of Science and Technology, Weiyang District, Xi'an, Shaanxi, 710021, China.
E-mail address: chenqingcai@sust.edu.cn (Q. Chen).

https://doi.org/10.1016/j.envres.2022.112899
Received 22 November 2021; Received in revised form 29 December 2021; Accepted 3 February 2022
Available online 14 February 2022

include adsorption and photochemical reactions.

The global coronavirus disease (COVID-19) outbreak posed a serious threat to public health (Wang et al., 2022). China as the first country to experience the COVID-19 pandemic, took the lead in carrying out epidemic control to protect people's lives and health in the whole world (Li et al., 2020; Wang et al., 2021). The quarantine city lockdown (CLD) measures by China's government included immediate lockdown of schools, offices, industries, and travel restrictions in order to control the spread of the pandemic (Wang and Zhang, 2021). The controlling pandemic measures lead to improve the air quality of China and other countries by reducing anthropogenic emissions and substantially decrease in human activity positively (Tobías et al., 2020). Although studies relating the influence of COVID-19 controlling measures on air quality have been prevalent in the past two years (Hong et al., 2021; Wang et al., 2020), but few studies have explored the toxicity of atmospheric particulate matter during the epidemic control. Therefore, the investigation to characterize the oxidative potential (OP), EPFRs and other chemical components are worthy to understand the toxicity change of particulate matter before and during CLD.

The present study is the first to investigate the influence of quarantine lockdown on the oxidative toxicity of fine particulate matter ($PM_{2.5}$) in Xi'an, China. The study conducted three weeks of observation from January 14 to February 3, 2020, with the same period in 2019. The oxidative stress level and EPFRs concentration were analyzed by electron paramagnetic resonance (EPR). Examining the EPFRs sources in Xi'an city is also helpful to understand the hazardous impact of EPFRs on the environment and formulate initiatives measures to control the air pollution from these sources. Moreover, the findings of this research will lead to enable the pathway for future studies on OP and EPFRs in $PM_{2.5}$.

2. Materials and method

2.1. Samples collection

Daily $PM_{2.5}$ samples were collected from January 14 to February 3, 2020, compared with the same period in 2019 at the Weiyang district of Xi'an, China. This sampling site is rooftop (>40 m above the ground level) of Shaanxi university of science and technology (34°22′35.07″N, 108°58′34.58″E). The samples were taken using a $PM_{2.5}$ high-volume sampler (XT-1025, Shanghai Xintuo, China). The collection of all samples started at 7:00 local time (Beijing time) and continued for 23 h 30 min. The samples were collected on a quartz filter (TISSUQUARTZ 2500QAT-UP, PALL, USA) and kept at −20 °C until further investigation. The flow rate was 1000 L/min. The daily $PM_{2.5}$ concentration were obtained from the Shaanxi provincial monitoring station at Shaanxi University of Science and Technology. In total, 42 atmospheric $PM_{2.5}$ samples were analyzed in this study.

2.2. Chemical compositions

The concentration of water-soluble ions (i.e., anions and cations), organic carbon (OC), and elemental carbon (EC) were carried out based on the methods briefly outlined below.

Water-soluble ions including Na^+, NH_4^+, K^+, Mg^{2+}, Ca^{2+}, F^-, Cl^-, NO_3^- and SO_4^{2-} analysis were performed on 12 mm filters via ultrasonic extraction with 15 mL of highly purified water, followed by filtering (PTFE filter, 0.45 μm). Finally, the level of these ions was determined through ion chromatography (940 Professional IC Vario, Metrohm) (Zhang et al., 2017).

The concentration of organic carbon (OC) and elemental carbon (EC) in $PM_{2.5}$ samples were determined by using an OC/EC analyzer (Model-4, Sunset Laboratory Inc.) with IMPROVE_A heating method detailed method is provided by Chen et al. (2019).

2.3. EPFR analysis and data processing

The EPR analysis of collected samples was determined by placing the quartz filters in an EPR spectrometer (MS5000, Freiberg Instruments Inc., Germany). G-factor calibration and absolute numbers of spins in collected samples were performed on standards containing Cr^{3+} and Mn^{2+} (Freiberg Instruments Inc., Germany). The EPR analysis was accomplished as described previously by Chen et al. (2018a). In this study, the established measuring parameters were set to scan time, 180 s; strength of the magnetic field, 330–345 mT; microwave power: 8 mW; modulation amplitude, 0.2 mT. Moreover, the concentration of EPFRs in the quartz filters was analyzed directly by using an EPR spectrometer.

The EPR signal for the samples was baseline corrected, and the Gaussian function was placed to fit the EPR signal. Later, the characteristic parameters of the EPFRs were obtained, including g-factor, ΔHp-p and peak height. The formula used to calculate the spin number is shown in Eq (1):

$$S_{EPRFs} = \overrightarrow{F} \times S_{Cr3+} \times \frac{A_{EPFRs}}{A_{Cr3+}} \quad (1)$$

where F represents the shape correction coefficient (1.06), S_{Cr3+} indicates the total chromium spin number, A_{EPFRs} and A_{Cr3+} presents the area of the integral curve in the EPR absorption curve of the sample and the chromium standard, respectively. The detailed methodology is described elsewhere (Chen et al., 2019).

2.4. Oxidative toxicity analysis

The dithiothreitol (DTT) assay is a popular noncellular method to measure the toxicity level in $PM_{2.5}$. In this process, the active oxygen consumes the DTT assay and is oxidized to produce disulfides. Consequently, this analysis is a quantitative evaluation of $PM_{2.5}$ to investigate the DTT consumption rate. In this study, the DTT consumption rate represents the concentration of ROS. The DTT activity detection was carried out the same as mentioned somewhere (Chen et al., 2019; Cho et al., 2005). Firstly, DTT assay was conducted by using the filter (5 mm) and 2 mL of ultra-pure water by vortexing (model MX-S, SCILOGEX, USA) for 5 min, followed by filtering (polytetrafluoroethylene filter, 0.45 μm). Secondly, the filtrate (0.5 mL) was mixed in DTT solution (0.5 mL, 1 mM DDT, ≥ 98%, Sigma-Aldrich, prepared with a phosphate buffer at pH = 7.4), and placed in a water bath at 37 °C, followed by sample collection at 0, 5, 10, 15, 25, and 40 min. Then, 1 mL trichloroacetic acid (1%, w/v) was added to stop the reaction, followed by a color reaction with 2 mL 0.08 M Tris buffer and 4 mM EDTA and 0.5 mL 0.2 mM 5,5′-dithiobis-(2-nitrobenzoic acid) (DTNB, ≥98%, Sigma-Aldrich). Finally, the absorbance of the sample at 409 nm was utilized using an ultraviolet–visible Spectrophotometer (AquaLog, HORIBA, Japan). The final DTT consumption rate (unit: μM/min) was calculated according to the measured absorbance at various time periods. The experiment was performed in the dark and measured absorbance was verified by detecting the solution absorbance by adding various DTT concentrations. The parallel analysis of the sample and background collected during the city lockdown provided in SI Fig. S5.

2.5. Source attributes with PMF

In this study, the factors contributing to EPFR in $PM_{2.5}$ were examined through the U.S. Environmental Protection Agency (EPA) source apportionment PMF model (version 5.0) (Hwang and Hopke, 2007; Zhang et al., 2008) To identify the sources, the total obtained results of PM_{10}, SO_2, $PM_{2.5}$, CO, O_3, NO_2, DTTv, and other chemical components (OC, EC, 9 water-soluble ions) were added in the PMF model (Brown et al., 2015; Paatero et al., 2014). This model enables estimation of the chemical concentration data such as signal-to-noise ratio (S/N) the specified importance of the chemicals (bad, weak, or strong) (Jaeckels

et al., 2007). In this model, the chemical concentrations below method detection limits (MDLs) are assumed to be excluded. The fundamental operation, imputation of uncertainties and missing values, and practical applications of PMF analysis and modeling can be found elsewhere (Reff et al., 2007; Xie et al., 2012).

3. Results and discussion

3.1. General overview of air quality

Epidemic control has significantly changed air quality and contributed to improved air quality by limiting production and transportation. Fig. 1a and b is demonstrating a total of 31 national and provincial control stations before the pandemic control (2020.01.20–2020.01.27) and during the CLD (2020.01.28–2020.02.03). During the pandemic, the weekly average $PM_{2.5}$ concentration decreased dramatically on a national scale. The time series comparison of air pollutants during the targeted time zone of 2019, 2020 and CLD is illustrated in Fig. 2a and b. The calculated mean value of $PM_{2.5}$ concentration from January 14 to February 3, 2019, was 87 μg/m^3 and showed a significant increase to150.85 μg/m^3 before the city lockdown (CLD). Conversely, a rapidly decreasing trend was observed during the CLD with a value of 72.85 μg/m^3. Moreover, the calculated concentrations of other air pollutants including PM_{10}, NO_2, SO_2, and CO showed significant variations while comparing 2019 and 2020, as demonstrated in Fig. 2c. The detailed information is likewise provided in Table S1. Comparatively these pollutants including PM_{10}, NO_2, SO_2, and CO presented a diminishing trend (by 84.73 μg/m^3, 24.63 μg/m^3, 0.89 μg/m^3, and 0.45 mg/m^3) during the CLD, while only O_3 increased (by 33.4 μg/m^3). As mentioned elsewhere,

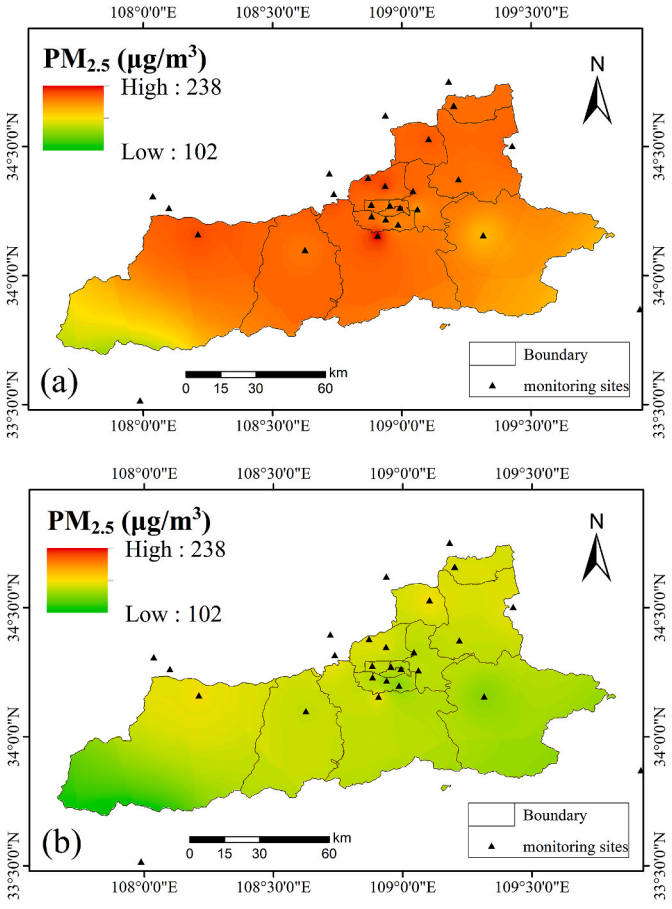

Fig. 1. Data source: Before and during the city lockdown (CLD) 31 national + provincial control stations (a) 2020.1.20–2020.1.27 weekly average $PM_{2.5}$ concentration; (b) 2020.1.28–2020.2.3 weekly average $PM_{2.5}$ concentration.

the reduced anthropogenic emission was observed in the temporal pattern of air pollutants during CLD. Other cities of China including Beijing, Wuhan, and Shanghai have reported similar results (He et al., 2020; Hong et al., 2021). During CLD, the local governments implied various controlling measures including restricting transport and public gatherings. Moreover, the industries were closed during this CLD. The higher concentration of O_3 during CLD was attributed to the reduction in NOx by increasing atmospheric oxidation and formation of secondary aerosols.

The satellite atmospheric overview also verified the reduction of these pollutant emissions during CLD. In China, Wuhan was the first city to adopt the lockdown measures and resulted in improved air quality. In our findings, the air quality in Xi'an improved significantly during the COVID-19 lockdown period. Thus, it can be stated that improved air quality attributed to controlling measures by the government of China during CLD. As mentioned elsewhere, secondary organic aerosol and combustion increased their contribution to $PM_{2.5}$. (Huang et al., 2021; Zheng et al., 2020).

3.2. Chemical composition of $PM_{2.5}$

In order to better understand the main factors influencing air quality during targeted time zoon in 2019, 2020, and CLD, this study analyzed the chemical compositions of $PM_{2.5}$, including WSIs, OC, and EC.

3.2.1. Water-soluble ions (WSIs)

Water-soluble ions (WSIs) as one of the major components of $PM_{2.5}$, it is valuable to understand the chemical characteristics and sources of $PM_{2.5}$. In this study, the water-soluble ions (WSIs) in $PM_{2.5}$ during the targeted time zone of 2019, 2020 and CLD is shown in Fig. 3a, Table S2. The mean of total WSIs concentrations in 2019, 2020 and CLD was 48.73 μg/m^3, 50.86 μg/m^3, and 34.15 μg/m^3, respectively. The most abundant ions including NH_4^+, NO_3^-, SO_4^{2-}, and Cl^- concentrations in the targeted time zone of 2019, 2020 and CLD were 10.23–14.29 μg/m^3, 14.78–15.01 μg/m^3, 11.05–15.52 μg/m^3, and 4.19–2.82 μg/m^3, respectively. While concentrations of Na^+, K^+, Mg^{2+}, Ca^{2+}, and F^- were relatively lower. During the CLD, the mean concentration of NH_4^+, NO_3^-, and SO_4^{2-} dropped dramatically from 14.29 μg/m^3 to 8.75 μg/m^3, 15.01 μg/m^3 to 9.33 μg/m^3, 15.52 μg/m^3 to 11.93 μg/m^3, respectively.

Moreover, the box plot in Fig. 3b is illustrating the total concentrations of WSIs in $PM_{2.5}$ in 2019, 2020 and CLD. The percentage of NO_3^- in 2019 was the biggest 30.3%, followed by SO_4^{2-} and NH_4^+ (22.7% and 21.0%). Significantly higher values of NO_3^- in winter can be assigned to local sources, such as traffic (Paraskevopoulou et al., 2015). During CLD, the lower concentrations of NH_4^+ and NO_3^- were attributed to the reduced flow of motor vehicles. During 2020, the concentration of SO_4^{2-} was high prior to the epidemic control and was probably caused by different anthropogenic activities, as well as poor dispersal of particles (He et al., 2020). However after the epidemic control, the concentration of SO_4^{2-} decreased first and then increased. During the CLD, SO_4^{2-} was the most abundant species with a proportion of 34.9% of total WSIs, followed by NH_4^+ and NO_3^- (25.6% and 27.3%) respectively. The relative increasing trend in SO_4^{2-} could be attributed to an increase in gaseous SO_2 emission due to coal-burning for heating system in winter (Hong et al., 2021).

According to Fig. 3c, the total percentage of WSIs concentrations in $PM_{2.5}$ during 2019 were 49%, others 51%. During 2020, before the pandemic control increased by 51%, others 49%. As a result, during the CLD, significantly decreased to 34%, with others 66% due to the reduction of the primary emissions.

3.2.2. Carbonaceous constituents (OC/EC)

The carbon component is an important part of atmospheric particulate matter and is responsible for the toxicity of particulate matter. Anthropogenic activities are the main reason for the high emissions of

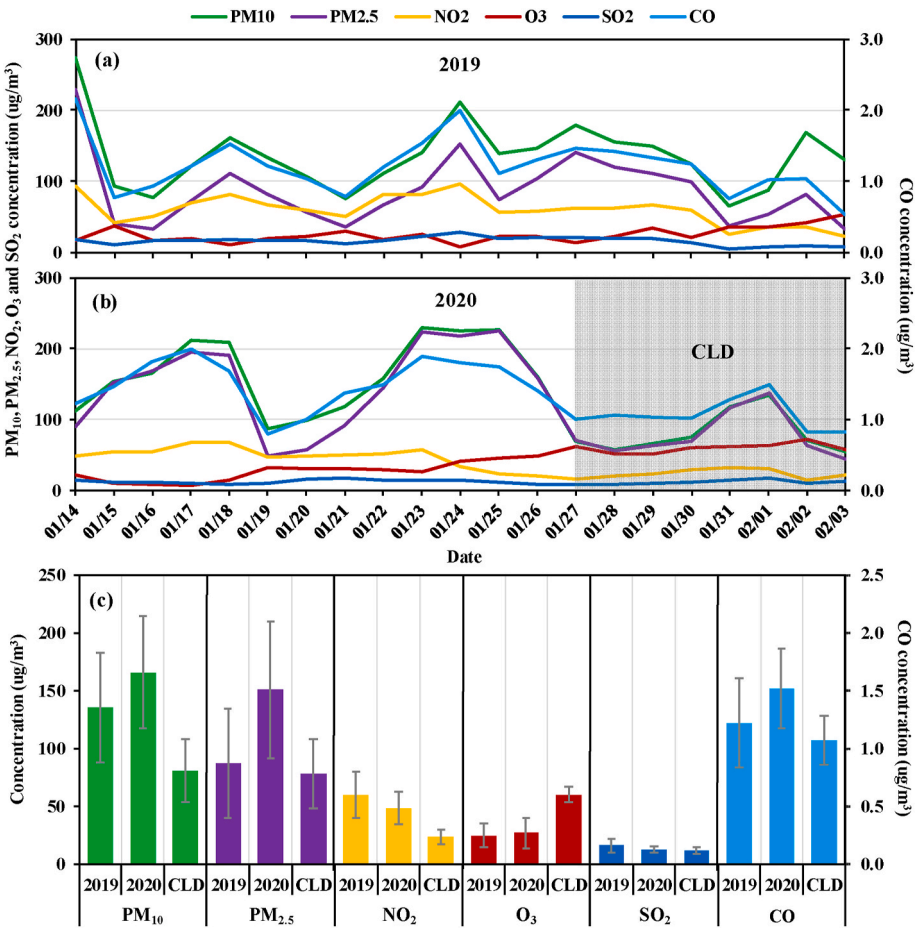

Fig. 2. Time series comparison of (a) air pollutants in 2019, (b) 2020 before the pandemic control and (c) during the city lockdown (CLD).

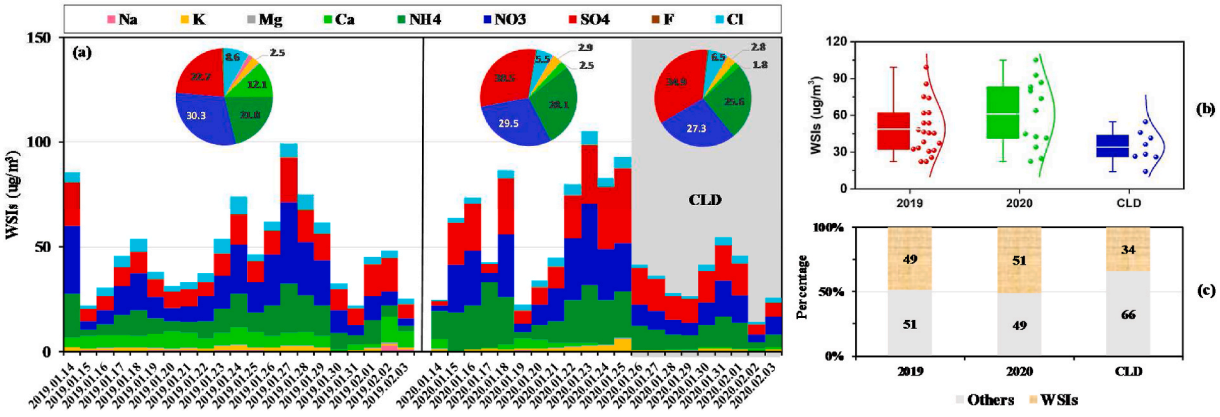

Fig. 3. Time series of water-soluble ions during targeted time zone in 2019, 2020, the city lockdown (CLD); (a) concentrations of water-soluble ions in $PM_{2.5}$; (b) total concentration of WSIs, (c) the percentage of WSIs in $PM_{2.5}$.

carbon aerosols, such as combustion emissions, motor vehicle emissions, and factory pollution emissions. The organic carbon (OC) (from primary emissions and secondary formation) (Huang et al., 2014) and elemental carbon (EC) from primary emissions (Bond et al., 2013) level and OC/EC ratio during targeted time zone in 2019, 2020 and CLD are demonstrated in Fig. 4a and b, Table S3.

Fig. 4c and d shows the total OC and EC level during 2019, 2020 and CLD were 33.73 ± 4.24 μg/m^3, 24.22 ± 1.67 μg/m^3 and 20.82 ± 1.47 μg/m^3, respectively. The OC/EC ratio is a significant indicator for assessing potential sources, such as biomass combustion and diesel or gasoline vehicle emissions. The mean OC/EC ratio in 2019 was 10.56, in 2020 before the pandemic control was 16.45, and during the CLD was 30.63 (OC/EC = 90), as illustrated in Fig. 4e. It shows that potential secondary organic aerosols are generated in large quantities. In this research, the OC and EC concentrations in 2020 and during the CLD (20.82 ± 1.47 μg/m^{3}and 24.22 ± 1.67 μg/m^3) were determined slightly lower than the time zone of 2019 (33.73 ± 4.24 μg/m^3) due to the control of air pollution sources, such as bulk coal burning and biomass burning Generally, OC/EC ratio is utilized to separate and characterize the sources of emissions. Normally, the higher value of OC/EC ratio

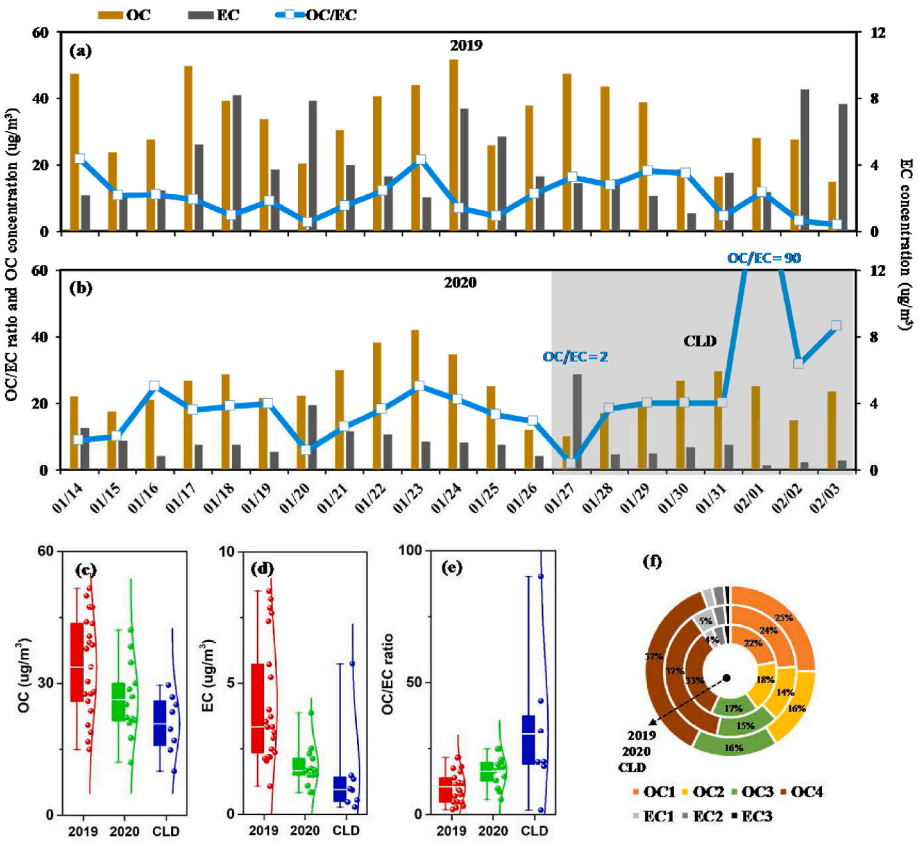

Fig. 4. OC and EC analysis during targeted time zone of 2019, 2020 and the city lockdown (CLD) (a, b) OC and EC concentrations in $PM_{2.5}$ and OC/EC ratio; (c) OC; (d) EC; (e) OC/EC ratio; (f) carbonaceous components (OC1-OC4; EC1-EC3).

leads to emissions through biomass burning, whereas the lower values lead to the dominance of emissions through fossil fuels (Chatterjee et al., 2021). In this study, the OC/EC ratio of 2020 compared to 2019 was higher, suggesting the reduced primary emissions and increased secondary aerosols in 2020. However, during the epidemic control (CLD), the EC compared to OC concentration showed a peak level at 5.74 μg/m^3, which demonstrates that combustion is the primary contributor, then rapid decrease was observed. Fig. 4f demonstrates the proportion of carbonaceous components (OC1-OC4; EC1-EC3) during the targeted time zone. The observed components OC1-OC4 during the CLD were much higher and EC1-EC3 were much lower than in 2019 and 2020, indicating the influence of secondary formation, which demonstrates that the reduced combustion emissions and atmospheric conditions in Xi'an is accountable for generation of more secondary organic matter.

3.3. EPFRs in $PM_{2.5}$

The COVID-19 controlled measures were expected to control the concentration and type of EPFRs in the atmosphere, as a novel health risk substance. EPFRs are mostly derived from combustion source, EC is the tracer of combustion source. The obtained concentration of EPFRs and EC in $PM_{2.5}$ from Xi'an during 2020 (before and CLD period) were significantly lower than the same period in 2019, as illustrated in Fig. 5a. EPFRs and EC trendlines are primarily used to compare the contribution of combustion sources. In detail, the mean atmospheric concentrations of EPFRs in $PM_{2.5}$ from January 14, 2020 to February 3, 2020 and January 14, 2019 to February 3, 2019 were 1.55×10^{14} spins/m^3 and 3.17×10^{14} spins/m^3. The obtained concentration of EPFRs during 2020 was approximately 1.62 times lower than the results of 2019. During the CLD, the concentration of EPFRs diminished more to 1.13×10^{14} spins/m^3. The obtained lower concentration of EPFRs during CLD was found 7.17×10^{13} spins/m^3 (1.28×10^{18} spins/g) on January 28, 2020. Conversely, the obtained highest concentration of EPFRs during CLD was 1.70×10^{14} spins/m^3 (1.45×10^{18} spins/g) on January 31, 2020. In our previous study, the EPFRs concentration during winter of 2017 was 3.17×10^{14} spins/m^3, which increased to a higher level as illustrated in present research (Chen et al., 2019). According to Xi'an Ecology and Environment Bureau 2018, haze episodes and central warming system could cause to EPFRs concentration in $PM_{2.5}$ in Xi'an city. The higher EPFRs concentration during 2019 can be attributed to these reasons. As mentioned elsewhere, the higher concentration of EPFRs during winters (ranged 1.0×10^{14} spins/m^3-2.92×10^{14} spins/m^3 ($PM_{2.5}$ range: 30–307 μg/m^3)) are highly associated with bad weather conditions and coal burning for central heating (Chen et al., 2018c). However, decreased EPFRs concentration were observed due to proper lockdown initiatives by Government. These results demonstrated that the replacement of coal-burning for heating and a series of special measures and policies at public living area can help to purify the air quality and reduced concentration of EPFRs.

In this study, the magnetic movement of EPFRs was identified by EPR spectra. The signal characteristics, g factor and ΔHp-p of EPFRs in atmospheric $PM_{2.5}$ samples during the targeted time zone are exemplified briefly in Table S4. According to the results, the calculated mean EPR spectra of EPFRs in atmospheric $PM_{2.5}$ samples during 2019 and 2020 were 2.0028 and 2.0030, respectively. The g factor of EPFRs in $PM_{2.5}$ samples during 2019 and 2020 was in the range of 2.0025–2.0033 and 2.0028 to 2.0033, respectively (Fig. 6a and b). During CLD, the EPR spectra were 2.0031, and the g factor was 2.0029–2.0032. In the comparative analysis of signal intensity, the end of 2019 and the start of 2020 including CLD presented weak signals. Conversely, strong signals were observed during the targeted time zone in 2019. The reason to explain the weak signals at the end of 2019 and the start of 2020 can be combustion source emissions are effectively controlled or the formation of secondary EPFRs is affected (Chen et al., 2018c). During CLD, the

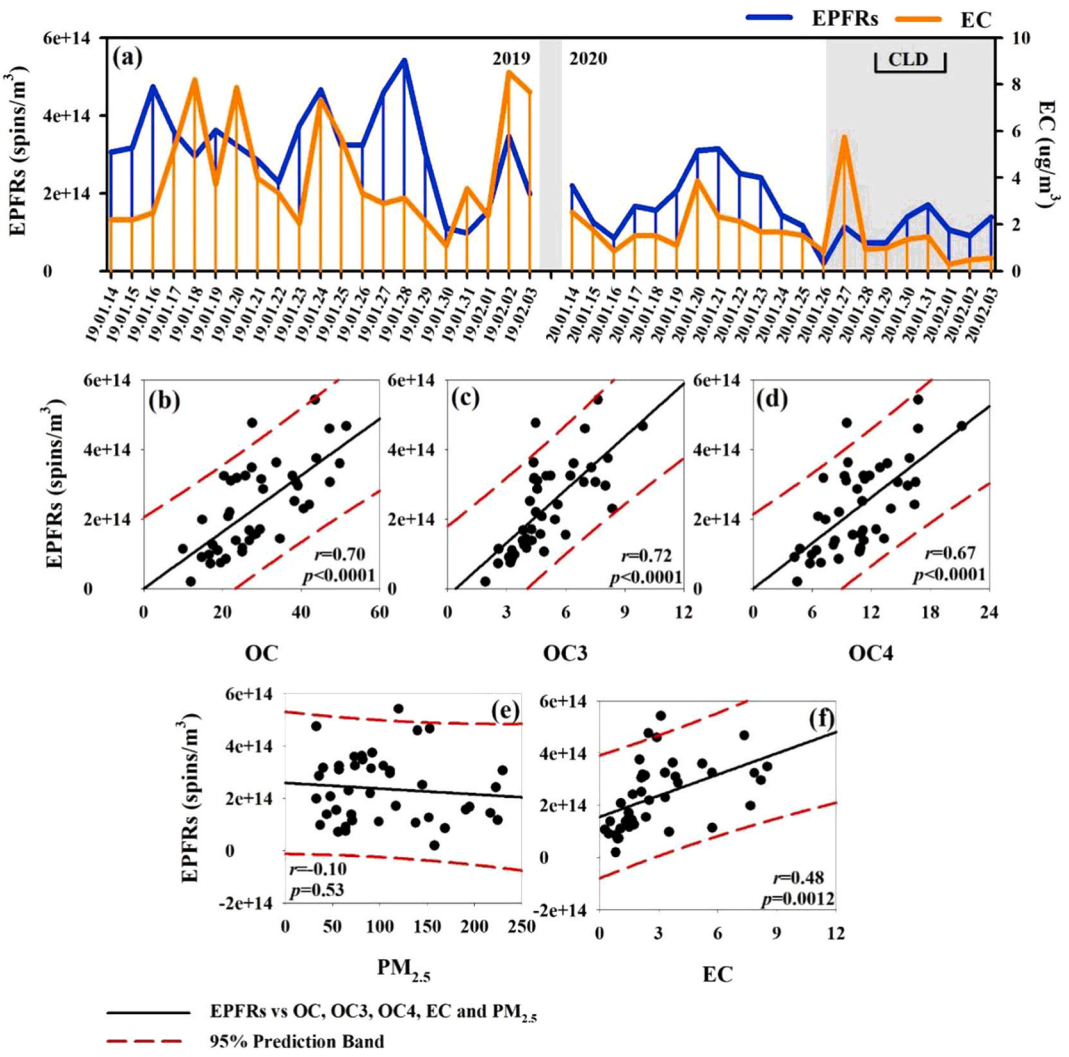

Fig. 5. Concentration of EPFR during targeted time zone in 2019, 2020, the city lockdown (CLD) (a) Comparisons of the EPFRs and EC concentration; Correlation analysis of EPFRs with (b) OC, (c) OC3, (d) OC4, (e) $PM_{2.5}$, and (f) EC.

lockdown control explains the weak signals of EPFRs. Generally, the value of g factor <2.0030 are associated to C-centered radicals, range 2.0030–2.0040 associated with a mixture of O- and C-centered radicals, and >2.0040 are associated with O-centered radicals (Ruan et al., 2019). Herein, substantially greater g factor during 2020 and CLD, as compared to 2019, indicating different types of EPFRs, it's probably an increase in the O-centered radicals. During CLD, the g factor <2.0030 presented that the EPFRs during this time zone belonged to carbon-centered radicals. The relative greater peak values indicated the probability of multiple radicals or a more robust matrix.

Compared with the $PM_{2.5}$ samples in 2019, before the pandemic control in 2020 and during the CLD, the EPFRs had a substantially greater g factor throughout the three weeks observation before and during the lockdown than the EPFRs in $PM_{2.5}$ in 2019, indicating that the types of EPFRs may be different (Chen et al., 2018a). Moreover, the highest obtained value of ΔHp-p of EPFRs in $PM_{2.5}$ was 6.2 G (range: 4.4–6.2), during CLD. The comparatively higher value of ΔHp-p likewise approved the presence of multiple organic radicals in $PM_{2.5}$ during CLD. Furthermore, the analyzed EPFRs in $PM_{2.5}$ during the CLD were long-lived organic free radicals.

The characterizing research to identify the factors that influence the EPFRs in the atmosphere is fundamental to take initiative against the health risks proposed by EPFRs. In this study, correlation analyses were adopted to analyze the relationship among the concentrations of common atmospheric pollutants (OC, OC3, OC4, EC, and $PM_{2.5}$) and EPFRs and to emphasize the environmental behaviors of EPFRs during the targeted time zone Figs. 5b, c, d, e, f, and S1, 2. The results presented a strong correlation between the EPFRs and OC3 ($r = 0.72$, $p < 0.0001$), OC ($r = 0.70$, $p < 0.0001$), OC4 ($r = 0.67$, $p < 0.0001$), and weak correlation with EC ($r = 0.48$, $p < 0.0012$). The strong relationship of EPFRs with OC3, OC4, and EC speculated that the formation of EPFRs might be from larger-molecular-weight and nonvolatile organic compounds (Chen et al., 2018b). Moreover, the positive correlation was observed inconsistently in between $PM_{2.5}$ and EPFRs Fig. S1. The ratio of average values between EPFRs and $PM_{2.5}$ concentrations shows the EPFRs/$PM_{2.5}$ ratio values are slightly lower during the CLD with a concentration of 1.59×10^{12} spins/m^3, than in 2019 (4.50×10^{12} spins/m^3) and 2020 (1.74×10^{12} spins/m^3). In general, the emission of $PM_{2.5}$ containing atmospheric primary particles is from power plants, vehicles, metallurgical plants. The formation of secondary particles is via the chemical and physical reaction of atmospheric components. Various scientists believe that the primary emission is a major source of EPFRs than secondary inorganic reaction (Wang et al., 2019). Consequently, it can be stated that the variation of sources and their role to $PM_{2.5}$ have a significant impact on the correlation of EPFRs and $PM_{2.5}$, suggesting the useability of EPFRs to determine the sources of $PM_{2.5}$ for the categorization of the emitted particles from vehicles and biomass/coal combustion.

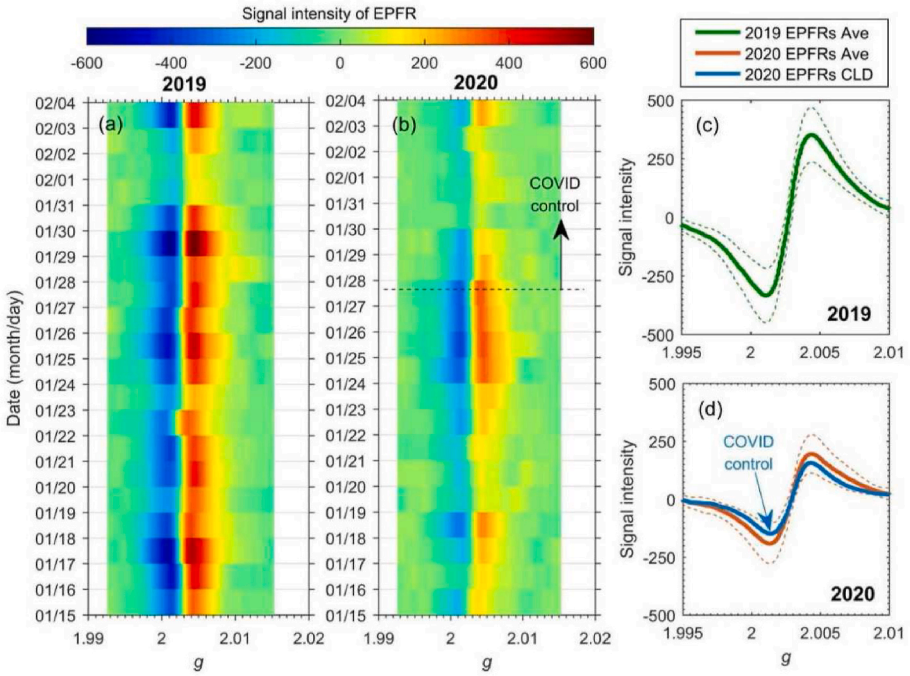

Fig. 6. EPR spectra during targeted time zone in 2019, 2020, the city lockdown (CLD) (a, b) average EPR spectra of the $PM_{2.5}$ samples. (c) the EPFR signal intensity and g-factor in 2019, (d) during 2020 and CLD.

3.4. Oxidation potential of $PM_{2.5}$

In this study, the DTT assay was optimized to quantify the OP of $PM_{2.5}$ during the targeted time. The OP of $PM_{2.5}$ samples was normalized by air volume (DTTv, nmol/min/m^3). Fig. 7 is shown the DTT activity levels in $PM_{2.5}$ during the targeted time zone of 2019, 2020 and CLD. During CLD, the quarantine measures were implied to slow down the spread of the virus. As illustrated in Fig. 7a, the DTT activity levels of $PM_{2.5}$ samples with atmospheric volume, and results showed that the average levels of DTTv during the targeted time zone of 2020 (4.32 nmol/min/m^3) was lower than in 2019 (4.78 nmol/min/m^3).

In contrast, the DTTv level during CLD increased to 4.38 nmol/min/m^3. During 2020, the concentration of $PM_{2.5}$ (150.85 μg/m^3) was significantly greater than the same time zone in 2019. However, a greater decreasing trend was observed in the concentration of $PM_{2.5}$ during the CLD period, but DTTv increased. The percentage of $PM_{2.5}$ per unit mass causes toxicity calculated by DTTv/$PM_{2.5}$ × 1000. As observed, the concentration of $PM_{2.5}$ was higher before the pandemic control and the toxicity level was lower. Consequently, the lower $PM_{2.5}$ concentration caused higher toxicity during the CLD period. During the pandemic, people spent all the time at home as instructed by the health departments. So, it can be stated that the causes air pollution was derived from the domestic interiors rather than the usual outdoor activities (Thakur et al., 2020). highlighted the toxic effect by increasing the rate of cooking and smoking at home due to the greater oxidative capacity of these particles. Other studies also enlisted the toxic effect of indoor activities such as cooking, household dust, smoke, candles, cigarettes (Lewis et al., 2020). Thus, indoor activities during CLD might be a reason for higher oxidative toxicity according to our view.

Fig. 8a demonstrates the average DTTv level in 2019 was higher with the concentration of 4.78 nmol/min/m^3 than before and during CLD (4.28 nmol/min/m^3, 4.38 nmol/min/m^3). To begin with, during the CLD the DTTv level was much higher than before the pandemic control. This explains why the toxicity level did not decrease during the lockdown period but rather increased. In addition, the EPFRs concentrations significantly reduced during the CLD compared to 2019 and 2020 concentrations, indicating a reduction in primary emissions Fig. 8b. Toxicity is caused by the percentage of $PM_{2.5}$ per unit mass, which can be calculated using DTTv/PM2.5 × 1000, as shown in Fig. 8c. According to our findings, the highest concentration of DTTv/$PM_{2.5}$ was in 2019. Before the pandemic control, $PM_{2.5}$ and toxicity level were lower. Despite this, during the CLD, the toxicity level sharply increased. Household emissions may have been a major contributor to the increased toxicity level during the city lockdown. Furthermore, during the CLD, both DTTv/EC ratio and EPFRs/EC ratio Fig. 8 e, f increased compared to 2019 and before the pandemic control. In conclusion, although motor vehicle emissions were reduced, burning coal contributed to an increase in toxicity.

The Spearman's correlation coefficient heat map between the DTTv with other pollutants and chemical components visualizes in Fig. 7b, as described above. In this study, the DTTv had the strong correlation with OC ($r = 0.7$), EPFRs ($r = 0.6$), SO_2 ($r = 0.6$), CL^- ($r = 0.6$), and moderate correlation with F^- ($r = 0.5$), weak correlation with CO, WSIs such as Ca^{2+}, NH_4^+, NO_3^- ($r = 0.3$), and weak negative correlation with O_3 ($r = -0.2$), and no positive correlation with $PM_{2.5}$, EC, Na^+ and SO_4^{2-} was observed as demonstrated in Fig. 7b.

In this study, the examined significant correlations between OP and OC were likewise approved in previous studies. Certain combustion sources such as biomass burning and coal combustion significantly contributed to waste soluble organic carbons are enlisted as a major contributor to OP (Fang et al., 2016) According to these results, the organic carbon (OC) made a significant contribution to the DTTv, which was consistent with previous research (Brehmer et al., 2019). In addition, there was a significant correlation between OP and EPFRs implying that EPFRs made contributions to the formation of these ROS species (Zhu et al., 2019) Fig. S3. Another study also showed that EPFRs concentration was positively correlated with DTTv, implying that the formation of ROS might be generated EPFRs. The EPFRs play a significant role catalyzing in the conversion of oxygen (O_2) to superoxide radicals (O_2^-) via electron transfer and the generation of hydrogen peroxide (H_2O_2) via disproportionation with hydrogen ions (H^+) and hydroxyl radicals (OH) through the Fenton reaction with ferrous ions (Fe^{2+}), according to Khachatryan and Dellinger (2011). SI provides the information about correlation analysis between DTTv with $PM_{2.5}$, OC, and EC

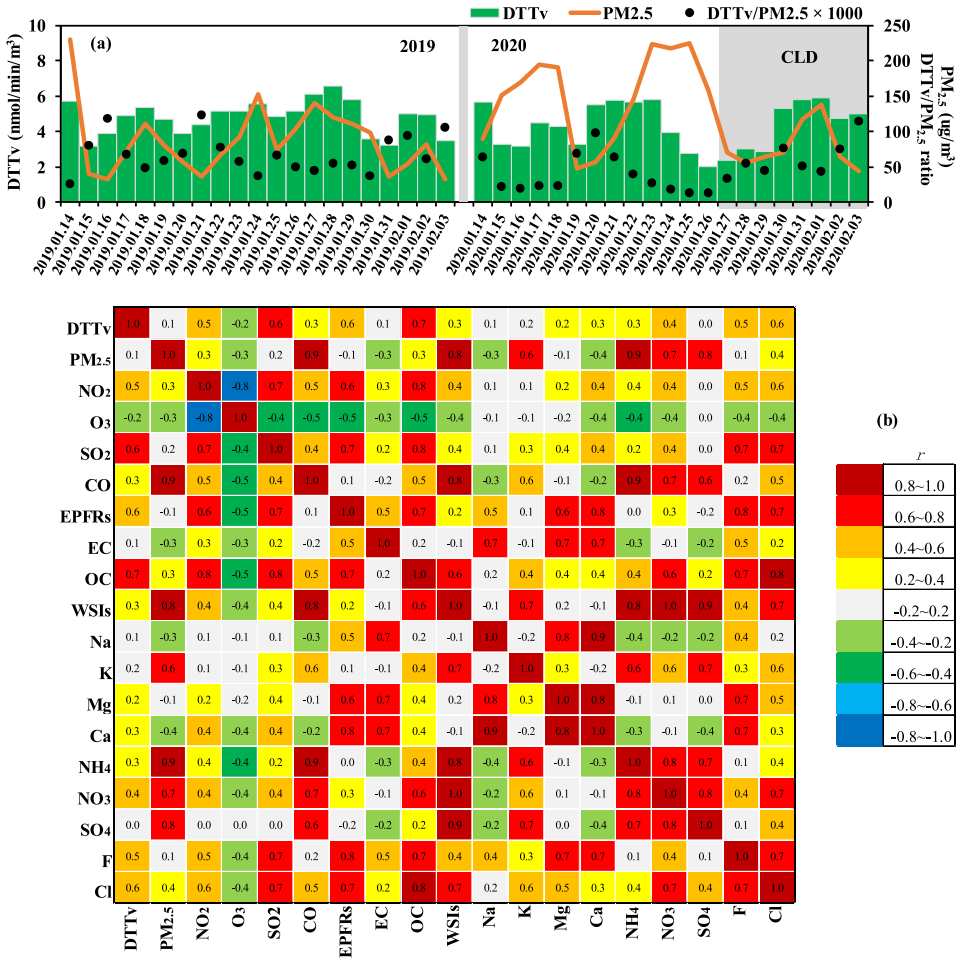

Fig. 7. DTT consumption rates during targeted time zone of 2019, 2020 and the city lockdown (CLD) (a) Comparative concentration of DTTv and $PM_{2.5}$, (b) correlation heat map of DTTv with other pollutants and compositions.

before and during the CLD, as compared in 2019 Fig. S4.

These findings suggested that the organic components are not the only contributor to induced oxidative toxicity; other $PM_{2.5}$ components, such as transition metals must have played a more active role to induce ROS activity (Xu et al., 2020).

3.5. *Source apportionment of $PM_{2.5}$, DTTv, EPFRs by PMF model*

The PMF model was used in our study to quantify the sources of $PM_{2.5}$, EPFRs, and DTTv before and during the city lockdown. Based on the factor contributions, coal combustion sources, photochemical oxidation, secondary aerosols, vehicle emissions, and dust were the main sources of $PM_{2.5}$, DTTv, and EPFRs during the targeted time (Figs. 9 and 10). Moreover, the percentage analysis of these resources is ascribed in Fig. 11.

Species such as OC, SO_2, NO_2, Cl^-, and K^+, as well as EPFRs, were dominant in the first factor with high proportions and identified as coal combustion sources (Kundu et al., 2010; Zhang et al., 2008) The detailed study about the contribution sources of $PM_{2.5}$ (ug/m^3) are described in Figs. S5, 6, 7, EPFRs (spins/m^3) contributions and percentages in Figs. S8 and 9, DTTv (nmol/min/m^3) in Figs. S10 and 11. In China, coal combustion is a prominent source for heating system, lasting nearly half a year. In the northern part of China, during the cold season, residential daily stir-frying activities for cooking and solid fuel (e.g., crop residues, wood, and coal) burning for heating are likewise significant combustion sources (Kong et al., 2015; Zheng et al., 2020). According to the results, the contribution of coal combustion to EPFRs in 2019 was comparatively lower (50.10%) than the same period in 2020 (62.06%). Moreover, a significant increasing trend was observed during CLD 64.24%. Conversely, in the case of coal combustion attributed to DTTv, a decreasing trend was observed in 2020 (42.49%) as compared to 2019 (57.16%), and further reduced during CLD (29.02%). According to this observation, it can be stated that coal combustion was the dominant source of EPFRs species and have less contribution to DTTv during the targeted time period.

The photochemical oxidation with a high concentration of O_3 was identified as factor 2. Secondary organic aerosols can be produced by the oxidation of Volatile Organic Compounds (VOC) by atmospheric oxidants such as ozone O_3, hydroxyl radicals OH, and nitrate radicals NO_3 (Fadel et al., 2021). Reduced nitrogen oxides caused O_3 enhancement, further facilitating the secondary aerosol formation and increased atmospheric oxidizing capacity (Le et al., 2020). Because of the significant contribution of traffic combustion sources in urban areas, NO_2 is frequently used as a tracer of road traffic emissions (Dutheil et al., 2020; Zoran et al., 2020). The emitted NOx contributes to the formation of secondary airborne pollutants like O_3 and $PM_{2.5}$. According to our results in the case of EPFRs, the increasing trend of photochemical oxidation attribution was observed from 2019 to 2020 (2.94–10.81%). Moreover, a significant increase was observed during CLD 28.81%. In the case of DTTv, the same increasing trend was observed in 2019 and 2020 (15.16%–34.40%) however increased more during CLD (62.12%). Thus, the contribution of photochemical oxidation was the main source of DTTv during the city lockdown.

High levels of EC, Na^+, Mg^{2+}, and Ca^{2+} are indicators of motor

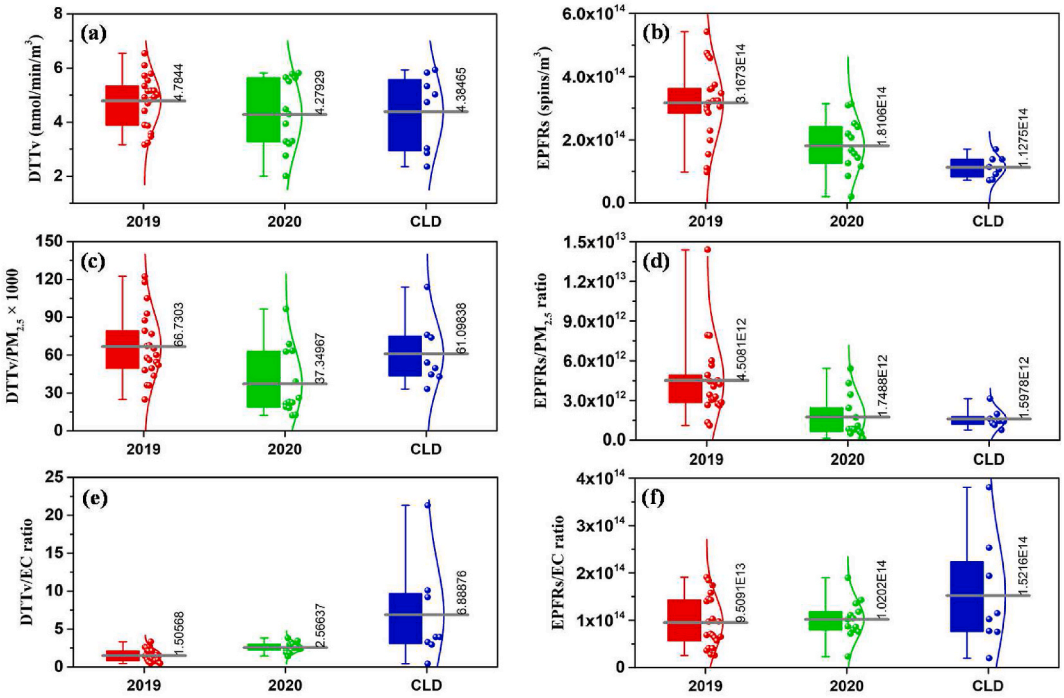

Fig. 8. Box-plot of the concentrations of DTTv nmol/min/m^3 (a), EPFRs spins/m^3 (b), DTTv/$PM_{2.5}$*1000 (c), EFPRs/$PM_{2.5}$ ratio (d), DTTv/EC ratio (e), and EPFRs/EC ratio (f) during 2019, 2020, and the city lockdown (CLD).

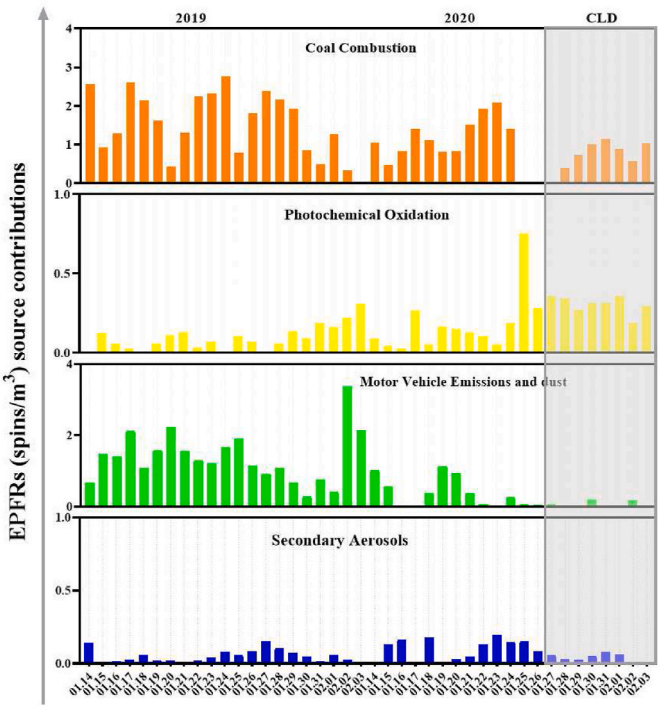

Fig. 9. Analysis of EPFRs source contributions by PMF model before and during the city lockdown (CLD). The bars represent the concentrations of various species to the factors.

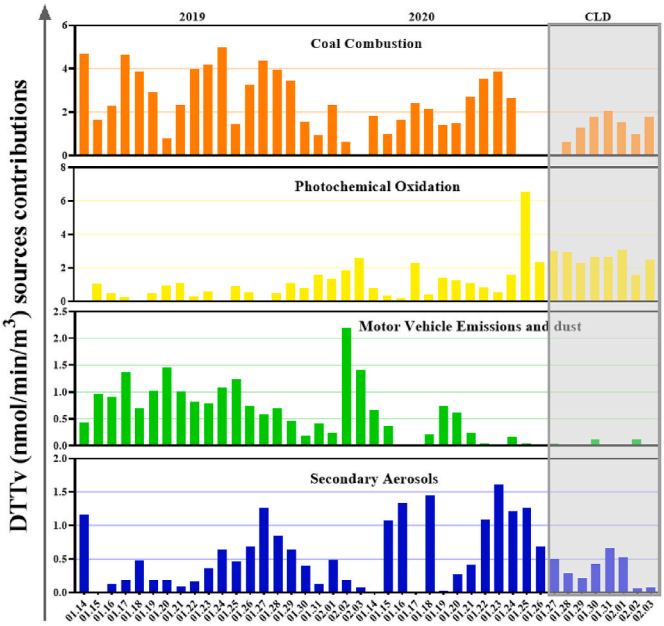

Fig. 10. Analysis of DTTv source contributions by PMF model before and during the city lockdown (CLD). The bars represent the concentrations of various species to the factors.

vehicle emissions and dust identified as Factor 3. A similar factor was resolved in previous studies, which was identified as vehicle emissions (Liu et al., 2018; Zheng et al., 2020). High levels of Mg^{2+} and Ca^{2+} were also identified as a dust source (An et al., 2015; Banerjee et al., 2015) In 2019, both EPFRs and DTTv contributions were significantly higher 45.30% and 18.51%. During CLD, the observed influence of motor vehicle emissions and dust on both EPFRs and DTTv was significantly reduced. The contribution to DTTv on motor vehicle emissions was nearly negligible (0.66%) during the CLD. Lockdown had a considerable impact on reduced vehicle travel resulting in less contribution of traffic both for EPFRs and DTTv, which had a significant effect on dust as well.

High sulfate and nitrate concentrations identify the presence of secondary aerosols. Factor 4 is distinguished as a secondary aerosol with high contributions of SO_4^{2-}, NO_3^-, and NH_4^+ (Liu et al., 2016; Zheng et al., 2020). Aside from their primary emissions from coal combustion

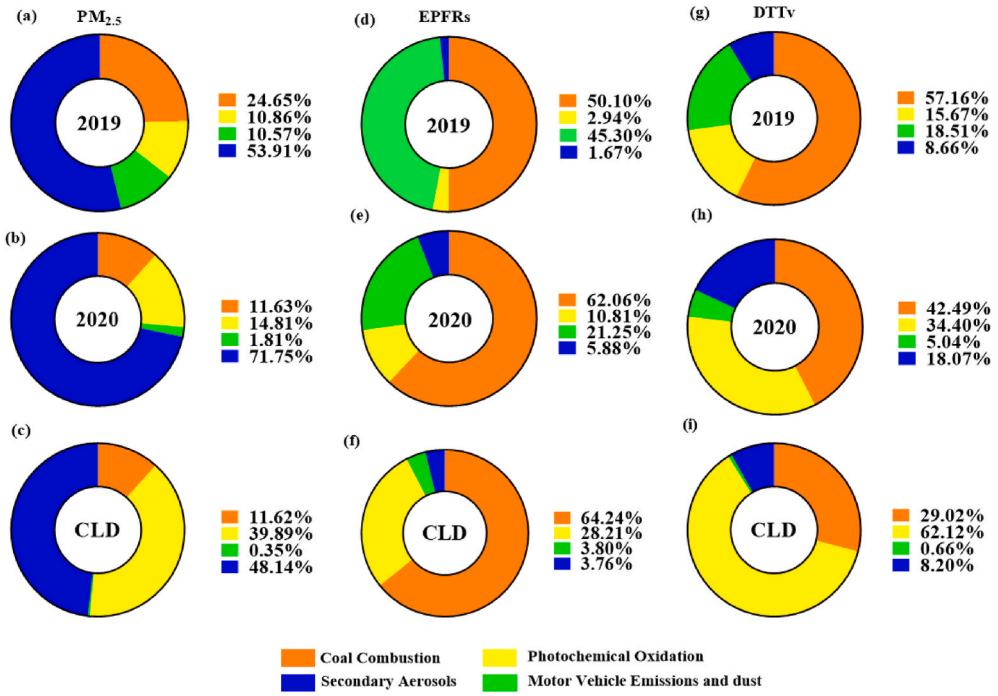

Fig. 11. Percentages of $PM_{2.5}$ contributions from different sources (a, b, c), EPFRs (e, f, g) and DTTv (g, h,i) in 2019, 2020 before the pandemic control and during the CLD.

(Dai et al., 2019; Yan et al., 2020), secondary aerosols can be produced by atmospheric homogenous and heterogeneous reactions (Seinfeld and Pandis, 2006). However, secondary sulfate, nitrate, and ammonium showed diminution during the CLD due to reduced emissions of SO_2 and NO_2. Decreased percentages of secondary aerosol attributed both to EPFRs and DTTv, according to the PMF analysis. During the CLD, secondary aerosols contribution to EPFRs was statistically insignificant, indicating less contribution by secondary aerosols. Consequently, DTTv contribution decreased by 8.20%, respectively. In another study, it was found that secondary sulfate and nitrate factors marginally influence the EPFRs (Wang et al., 2019). In our study, we have found that both EPFRs and DTTv barely contribute to secondary aerosols contributions.

4. Conclusion

On the basis of chemical components and a PMF model, we analytically figured the characterization and sources of toxic substances including $PM_{2.5}$, EPFRs, and other pollutants that cause oxidative potential and impact during the pandemic lockdown over Xi'an city. Compared to the same period in 2019, the average concentrations of various air pollutants, including PM_{10}, $PM_{2.5}$, NO_2, SO_2, and CO, clearly reduced by 2%–22%, whereas only O_3 increased by 30%. The higher concentration of O_3 during CLD was attributed to the reduction in NOx by increasing atmospheric oxidation and formation of secondary aerosols. The main chemical components of $PM_{2.5}$, WSIs, OC and EC, during the city lockdown also diminished by 17%, 5%, and 3% as a result of anthropogenic emission reductions. Due to pandemic measures, the quality of air improved all over China. However, the oxidative potential increased excessively as compared with the same period in 2019. Secondary emissions, coal combustion were major identified factors affecting the toxicity of the pollutants in Xian city. The obtained concentration of EPFRs during 2020 was approximately lower than the results of 2019. During the CLD, the concentration of EPFRs diminished more by 12%. During CLD, the g factor <2.0030 presents that the EPFRs belonged to carbon-centered radicals. Furthermore, the analyzed EPFRs in $PM_{2.5}$ during the CLD were long-lived organic free radicals. By comparing the OP level of $PM_{2.5}$ in Xi'an before and during the city lockdown, the OP level of $PM_{2.5}$ during the lockdown was deemed to be significantly higher than before the pandemic control, whereas the concentration of $PM_{2.5}$ was lower. The PMF analysis determined that coal combustion (64.24%) contributed significantly to EPFRs during the CLD by cause of heating systems, emphasizing the importance of coal combustion for EPFRs over other influencing factors. The contribution of photochemical oxidation to $PM_{2.5}$, EPFRs, and DTTv increased significantly by 39.89%, 28.21%, and 62.12%, while motor vehicle emissions and dust decreased dramatically, indicating a reduction in anthropogenic emissions. Factors of the secondary nitrate and secondary sulfate barely contributed both to EPFRs (3.76%) and DTTv (8.20%), while $PM_{2.5}$ (48.14%) showed significant contribution due to complete lockdown. The city lockdown, however, had a positive impact on the environment, although no significant health benefits were observed. However, it was suggested that the increased secondary formation of $PM_{2.5}$ was a significant source of toxicity.

Based on the aforementioned results, recommendations for future research are to visualize the formation pathway of OP and EPFRs from secondary emissions. Furthermore, future research should focus on the formation of EPFRs and OP in $PM_{2.5}$ by coal combustion and increased oxidation in the atmosphere. Finally, strategical measures to control the adverse health effect on human health by toxicity of EPFRs and OP induced by atmospheric particulate matter should be clearly highlight in future studies.

Author contributions

DA and QC designed the experiments and data analysis. YW performed PMF analysis. Hao Li and Hao Lin performed EPR analysis. XM and XX performed the spatial analysis. DA and QC prepared the paper with the contributions from all co-authors.

Declaration of competing interest

The authors declare that they have no known competing financial interests or personal relationships that could have appeared to influence the work reported in this paper.

Acknowledgements

This research was supported by grants from the National Natural Science Foundation of China (41877354) and the Youth Science and Technology Nova Program of Shaanxi Province (2021KJXX-36).

Appendix A. Supplementary data

Supplementary data to this article can be found online at https://doi.org/10.1016/j.envres.2022.112899.

References

An, J., et al., 2015. Fine particulate pollution in the Nanjing northern suburb during summer: composition and sources. Environ. Monit. Assess. 187, 1–14.
Banerjee, T., et al., 2015. Source apportionment of airborne particulates through receptor modeling: Indian scenario. Atmos. Res. 164, 167–187.
Bond, T.C., et al., 2013. Bounding the role of black carbon in the climate system: a scientific assessment. J. Geophys. Res. Atmos. 118, 5380–5552.
Brehmer, C., et al., 2019. The oxidative potential of personal and household PM2. 5 in a rural setting in southwestern China. Environ. Sci. Technol. 53, 2788–2798.
Brown, S.G., et al., 2015. Methods for estimating uncertainty in PMF solutions: examples with ambient air and water quality data and guidance on reporting PMF results. Sci. Total Environ. 518, 626–635.
Chatterjee, A., et al., 2021. High rise in carbonaceous aerosols under very low anthropogenic emissions over eastern Himalaya, India: impact of lockdown for COVID-19 outbreak. Atmos. Environ. 244, 117947.
Chen, Q., et al., 2019. Characteristics of environmentally persistent free radicals in PM2. 5: concentrations, species and sources in Xi'an, Northwestern China. Environ. Pollut. 247, 18–26.
Chen, Q., et al., 2018a. Dominant fraction of EPFRs from nonsolvent-extractable organic matter in fine particulates over Xi'an, China. Environ. Sci. Technol. 52, 9646–9655.
Chen, Q., et al., 2018b. Enhanced health risks from exposure to environmentally persistent free radicals and the oxidative stress of PM2. 5 from Asian dust storms in Erenhot, Zhangbei and Jinan, China. Environ. Int. 121, 260–268.
Chen, Q., et al., 2018c. Rapid determination of environmentally persistent free radicals (EPFRs) in atmospheric particles with a quartz sheet-based approach using electron paramagnetic resonance (EPR) spectroscopy. Atmos. Environ. 184, 140–145.
Cho, A.K., et al., 2005. Redox activity of airborne particulate matter at different sites in the Los Angeles Basin. Environ. Res. 99, 40–47.
Dai, Q., et al., 2019. Residential coal combustion as a source of primary sulfate in Xi'an, China. Atmos. Environ. 196, 66–76.
Dutheil, F., et al., 2020. COVID-19 as a factor influencing air pollution? Environ. Pollut. 263, 114466.
Fadel, M., et al., 2021. PM2. 5 characterization of primary and secondary organic aerosols in two urban-industrial areas in the East Mediterranean. J. Environ. Sci. 101, 98–116.
Fang, T., et al., 2016. Oxidative potential of ambient water-soluble PM 2.5 in the southeastern United States: contrasts in sources and health associations between ascorbic acid (AA) and dithiothreitol (DTT) assays. Atmos. Chem. Phys. 16, 3865–3879.
He, G., et al., 2020. The short-term impacts of COVID-19 lockdown on urban air pollution in China. Nat. Sustain. 3, 1005–1011.
Hong, Y., et al., 2021. Source apportionment of PM2. 5 and sulfate formation during the COVID-19 lockdown in a coastal city of southeast China. Environ. Pollut. 117577.
Huang, X., et al., 2021. Enhanced secondary pollution offset reduction of primary emissions during COVID-19 lockdown in China. Natl. Sci. Rev. 8, nwaa137.
Huang, X.H., et al., 2014. Contributions of vehicular carbonaceous aerosols to PM 2.5 in a roadside environment in Hong Kong. Atmos. Chem. Phys. 14, 9279–9293.
Hwang, I., Hopke, P.K., 2007. Estimation of source apportionment and potential source locations of PM2. 5 at a west coastal IMPROVE site. Atmos. Environ. 41, 506–518.
Jaeckels, J.M., et al., 2007. Positive matrix factorization (PMF) analysis of molecular marker measurements to quantify the sources of organic aerosols. Environ. Sci. Technol. 41, 5763–5769.
Khachatryan, L., Dellinger, B., 2011. Environmentally persistent free radicals (EPFRs)-2. Are free hydroxyl radicals generated in aqueous solutions? Environ. Sci. Technol. 45, 9232–9239.
Kong, S., et al., 2015. The relationship between the dust and gas-phase co across the California molecular cloud. Astrophys. J. 805, 58.
Kundu, S., et al., 2010. Diurnal variation in the water-soluble inorganic ions, organic carbon and isotopic compositions of total carbon and nitrogen in biomass burning aerosols from the LBA-SMOCC campaign in Rondônia, Brazil. J. Aerosol Sci. 41, 118–133.
Le, T., et al., 2020. Unexpected air pollution with marked emission reductions during the COVID-19 outbreak in China. Science 369, 702–706.
Lewis, A., et al., 2020. Estimation of Changes in Air Pollution Emissions, Concentrations and Exposure during the COVID-19 Outbreak in the UK.
Li, Q., et al., 2020. Early transmission dynamics in Wuhan, China, of novel coronavirus–infected pneumonia. N. Engl. J. Med.
Liu, T., et al., 2016. Formation of secondary aerosols from gasoline vehicle exhaust when mixing with SO 2. Atmos. Chem. Phys. 16, 675–689.
Liu, W., et al., 2018. Oxidative potential of ambient PM2. 5 in the coastal cities of the Bohai Sea, northern China: seasonal variation and source apportionment. Environ. Pollut. 236, 514–528.
Paatero, P., et al., 2014. Methods for estimating uncertainty in factor analytic solutions. Atmos. Meas. Tech. 7, 781–797.
Paraskevopoulou, D., et al., 2015. Sources of atmospheric aerosol from long-term measurements (5 years) of chemical composition in Athens, Greece. Sci. Total Environ. 527, 165–178.
Qian, R., et al., 2020. Characteristics and potential exposure risks of environmentally persistent free radicals in PM2. 5 in the three gorges reservoir area, Southwestern China. Chemosphere 252, 126425.
Reff, A., et al., 2007. Receptor modeling of ambient particulate matter data using positive matrix factorization: review of existing methods. J. Air Waste Manag. Assoc. 57, 146–154.
Ruan, X., et al., 2019. Formation, characteristics, and applications of environmentally persistent free radicals in biochars: a review. Bioresour. Technol. 281, 457–468.
Seinfeld, J.H., Pandis, S.N., 2006. Atmospheric Chemistry and Physicsfrom Air Pollution to Climate Change.
Thakur, M., et al., 2020. Biomass use and COVID-19: a novel concern. Environ. Res. 186, 109586.
Tobías, A., et al., 2020. Changes in air quality during the lockdown in Barcelona (Spain) one month into the SARS-CoV-2 epidemic. Sci. Total Environ. 726, 138540.
Vejerano, E.P., et al., 2018. Environmentally persistent free radicals: insights on a new class of pollutants. Environ. Sci. Technol. 52, 2468–2481.
Wang, Q., et al., 2022. Impact of COVID-19 pandemic on oil consumption in the United States: a new estimation approach. Energy 239, 122280.
Wang, Q., et al., 2021. Integrating digital technologies and public health to fight covid-19 pandemic: key technologies, applications, challenges and outlook of digital healthcare. Int. J. Environ. Res. Publ. Health 18, 6053.
Wang, Q., Zhang, F., 2021. What does the China's economic recovery after COVID-19 pandemic mean for the economic growth and energy consumption of other countries? J. Clean. Prod. 295, 126265.
Wang, Y., et al., 2019. Source apportionment of environmentally persistent free radicals (EPFRs) in PM2. 5 over Xi'an, China. Sci. Total Environ. 689, 193–202.
Wang, Y., et al., 2020. Changes in air quality related to the control of coronavirus in China: implications for traffic and industrial emissions. Sci. Total Environ. 731, 139133.
Xie, M., et al., 2012. Positive matrix factorization of PM2. 5: comparison and implications of using different speciation data sets. Environ. Sci. Technol. 46, 11962–11970.
Xu, Y., et al., 2020. Risk evaluation of environmentally persistent free radicals in airborne particulate matter and influence of atmospheric factors. Ecotoxicol. Environ. Saf. 196, 110571.
Yan, Q., et al., 2020. Emission and simulation of primary fine and submicron particles and water-soluble ions from domestic coal combustion in China. Atmos. Environ. 224, 117308.
Zhang, C., et al., 2017. Aerosol chemical characteristics for different air pollution levels in North Suburban Nanjing. Huan jing ke xue= Huanjing kexue 38, 4932–4942.
Zhang, Y., et al., 2008. Source apportionment of in vitro reactive oxygen species bioassay activity from atmospheric particulate matter. Environ. Sci. Technol. 42, 7502–7509.
Zheng, M., et al., 2020. Understanding sources of fine particulate matter in China. Philos. Trans. Royal Soc. A 378, 20190325.
Zhu, K., et al., 2019. Formation of environmentally persistent free radicals on microplastics under light irradiation. Environ. Sci. Technol. 53, 8177–8186.
Zoran, M.A., et al., 2020. Assessing the Relationship between Ground Levels of Ozone (O3) and Nitrogen Dioxide (NO2) with Coronavirus (COVID-19) in Milan, Italy, vol. 740. Science of The Total Environment, p. 140005.